Journal of Colloid and Interface Science **247,** 33–46 (2002)
doi:10.1006/jcis.2001.8095, available online at http://www.idealibrary.com on IDEAL®

Cluster–Cluster Aggregation Kinetics and Primary Particle Growth of Soot Nanoparticles in Flame by Light Scattering and Numerical Simulations

Stefano di Stasio,*,[1] Athanasios G. Konstandopoulos,† and Margaritis Kostoglou†

*Istituto Motori C.N.R., Via Marconi 8, 80125 Napoli, Italy; and †CERTH/CPERI, 6th Km. Charilaou-Thermi Road P.O. Box 361, 57001 Thermi Thessaloniki, Greece

Received June 13, 2001; accepted November 8, 2001

The agglomeration kinetics of growing soot generated in a diffusion atmospheric flame are here studied *in situ* by light scattering technique to infer cluster morphology and size (fractal dimension D_f and radius of gyration R_g). SEM analysis is used as a standard reference to obtain primary particle size D_P at different residence times. The number N_P of primary particles per aggregate and the number concentration n_A of clusters are evaluated on the basis of the measured angular patterns of the scattered light intensity. The major finding is that the kinetics of the coagulation process that yields to the formation of chain-like aggregates by soot primary particles (size 10 to 40 nm) can be described with a constant coagulation kernel $\beta_{c,\mathrm{exp}} = 2.37 \times 10^{-9}$ cm^3/s (coagulation constant $\tau_c \approx 0.28$ ms). This result is in nice accord with the Smoluchowski coagulation equation in the free molecular regime, and, vice versa, it is in contrast with previous studies conducted by invasive (*ex situ*) techniques, which claimed the evidence in flames of coagulation rates much larger than the kinetic theory predictions. Thereafter, a number of numerical simulations is implemented to compare with the experimental results on primary particle growth rate and on the process of aggregate reshaping that is observed by light scattering at later residence times. The restructuring process is conjectured to occur, for not well understood reasons, as a direct consequence of the atomic rearrangement in the solid phase carbon due to the prolonged residence time within the flame. Thus, on one side, it is shown that the numerical simulations of primary size history compare well with the values of primary size from SEM experiment with a growth rate constant of primary diameter about 1 nm/s. On the other side, the evolution of aggregate morphology is found to be predictable by the numerical simulations when the onset of a first-order "thermal" restructuring mechanism is assumed to occur in the flame at about 20 ms residence time leading to aggregates with an asymptotic fractal dimension $D_{f,\infty} \approx 2.5$.

Key Words: **soot; nanoparticles; kinetics; agglomeration; surface growth; fractals; light scattering.**

1. INTRODUCTION

Flame route can be implemented to generate nanoparticle aggregates of different nature (1–4). The structure of these multi-spherule aggregates is recognized to be fractal-like (3–6), namely they exibit a power law between the scaling of cluster mass and size. A power law also exists within such aggregates between radial position and solid fraction (7). These correlations are usually observed within a limited range of length scales that spans from the mean size of the primary sub-units (lower cut-off) to the so-called correlation length (upper cut-off) of the aggregates (8, 9). Plenty of works are reported in the recent literature about joint experimental and numerical studies on the kinetics of aggregation and surface growth of nanoparticles and aggregates (10–18).

Historically, the early contribution in the field of coagulation kinetics for binary hard-sphere interactions was made by Smoluchowski (19) who investigated the coalescence of liquid droplets. Smoluchowski's approach to model the time evolution of the number concentration $n(t)$ was based on the main underlying assumptions that the collisions between the particles undergoing Brownian motion are binary and that the fluctuations of density in the medium are sufficiently small in order to retain the randomness of the collisions. The balance equation, introduced by this author, accounted uniquely for the net removal of spherical particles due to coagulation and neglected any term of loss, such as evaporation, or generation of fresh particles. In this approach the number of collisions per unit time between particles is not depending on particle volume and all the collision are assumed to be effective, namely to result in the sticking of the particles undergoing collision. Thus, the balance equation was written as $dn/dt = -\frac{1}{2}K_c n^2$ and the coagulation costant K_c was evaluated according to Einstein's diffusion theory. The first report describing the aerosol balance in terms of integrodifferential equation was given by Muller (20) and it was later corrected by Schuman (21) and Zebel (22). Successive studies were addressed to account for loss and gain of particles in the formulation of the so-called general Dynamic Equation (GDE). Thus, for example, Friedlander (23) reported in the balance equation

[1] To whom correspondence should be addressed. E-mail: s.distasio@motori.im.na.cnr.it.

0021-9797/02 $35.00

a term describing the rate of growth of an individual particle due to the evaporation or condensation. The effects of the electrical charge on the balance equation have been studied by several authors among which Gillespie (24) and Rosinski *et al.* (25).

The coagulation process can be described in terms of the number distribution function $n(t)$ that represents the number of the aerosol particles per unit volume with individual volume in the range v to $v + dv$. The rate at which a particle of volume u undergoes coagulation with another particle of volume v, is termed the collision frequency and it is written as $\beta_c(u, v)\, n(u)\, n(v)$, where $\beta_c(u, v)$ is called the coagulation kernel or the collision kernel and has the dimensions of length cubed times inverse time. Expressions for the collision kernel describing the coagulation process in the limit of free molecular regime (particle with radius r very small with respect to the mean free path λ of molecules in the surrounding gas) and continuum regime ($r \gg \lambda$) are reported by Lai *et al.* (26) and Hidy (27), respectively. Extended reviews are authored by Friedlander (23), Mountain *et al.* (28), Williams and Loyalka (29).

Several works in the literature of the 1970s (30, 31) investigated the coagulation of carbon particles in flames as effect of Van der Waals attraction and particle charging. These authors used invasive methods, such as molecular beam sampling, and the subsequent electron microscopy analysis to measure particle size distributions, number concentration, and fraction of particles charged at different residence times. They found extremely high coagulation rates, exceeding a factor 10 the predictions on kinetic theory collisions. These unusually high coagulation rates were not explained in those works. In any case, these investigations suffer from the recognized fact that sampling can modify or hinder the measurement of the physical properties of particles in a flame, especially with concern to the kinetics of the process.

Observation of enhancements of coagulation rates has been previously reported (32, 33) for nanoparticles of different nature (NaCl, ZnCl2, Ag).

Some authors (34) reported the enhancement in the coagulation rate between agglomerates depending on their morphological properties. As a matter of fact, the diffusion properties of a cluster of nanoparticles are significantly different from that of a sphere at parity of mass (35). Other more recent papers have sustained the evidence that very strong attractive energy (36) and force interactions (37) do exist during the process of sticking between fractal aggregates. In particular, attractive energy is reported to be several orders of magnitude stronger with respect to that computed from the Hamaker equation (38) and attractive long-range forces are demonstrated to exist during the process of sticking of soot aggregates, probably explainable on the basis of electric charge effects. From the above consideration follows the necessity to further investigate the agglomeration kinetics and the coagulation rates within the process of fractal-like cluster formation by nanoparticle. For soot aggregates, surface growth and oxidation should be considered to occur in parallel with the main agglomeration process. Prediction for the size of primary TiO_2 particles undergoing collision and coalescing is reported by Lehtinen *et al.* (39) before the onset of dendrite (necking) between them.

Fractal aggregates of spherules can also undergo sintering or restructuring that depends on characteristics times and flow properties (16, 17, 40). The rearrangement of the aggregate structure is usually explained in terms of surface free-energy minimization (36), thermal settlement (41), surface diffusion (42, 16), effect of the shear flow (43), and capillary driven viscous flows (44).

Numerical models based on Monte Carlo simulations have been recently reported to apply to such mechanisms (40, 45). It should also be stressed that particle shape is expected to significantly influence the transport properties (14). There is strong interest in the scientific community about experimental and numerical studies on the formation and evolution of multi-spherule aggregates generated in flames in view of the attractive possibility to accurately control the properties of nanostructured materials synthesized via the combustion route.

The aim of this paper is to report the results of a joint experimental and numerical study on the kinetics of the coagulation process leading to evidence of a restructuring process for nanoparticle soot aggregates in a diffusion flame at atmospheric pressure. Time history of the aggregate morphology and aggregate number concentrations are obtained in the experiments by the application of a noninvasive light scattering technique. The use of probing is restricted solely to evaluating below a standard modality the mean size of soot primary particles (subunits constituting soot aggregates) at different times by scanning electron microscopy (SEM) analysis. Light scattering measurements have been also demonstrated in previous work (46) to be useful to compliment microscopy analysis with the aim of primary particle size estimation. Particular enphasis is here placed on the rates of the agglomeration process and on the surface growth mechanism of the primary particles. Computations are performed to investigate the predictibility of the mechanism of the agglomerate reshaping observed in the experiments. The evolution of aggregate size and fractal dimension is described during Brownian coagulation by a multivariate population dynamics approach introduced in recent work (47). The coagulation kernel β_c and the particle surface growth rate K_G are evaluated on the basis of the experimental work without any *a priori* assumption about the physical and chemical properties of particles (like refractive index, shape, morphology, etc.).

The paper is organized as follows. A theoretical framework is outlined in Section 2 to describe analytically the mechanisms of coagulation between fractal clusters in the free molecular and continuum regimes. The experimental results obtained *in situ* by the application of light scattering techniques are summarized in Section 3. Measurements of the copolarized scattered light intensity are performed at different polar angles θ. Reduction of the experimental data is made with a standard procedure to infer the fractal dimension, gyration radius, mean number of particles per aggregates, volume fraction, and weight of the aggregates at different residence times. The growth rates of the primary

soot spheroids are deduced experimentally by image analysis of the scanning electron microscopy micrographs of soot samples taken directly in flame at different residence times. Simulations are then performed by implementing the bivariate coagulation equation with independent variables the size and fractal dimension of the aggregates. The results are described in Section 4. In particular, simulations include the growth of primary spherules, as obtainable by the condensation of matter from the gas phase, and the time evolution of aggregate fractal dimension. The reshaping of aggregates observed in the light scattering experiments is also modeled in simulations introducing a "thermal" restructuring mechanism and following its effects on the joint size–fractal dimension aggregate distribution. For both growth rate of primary particles and fractal dimension, a comparison is made between the experimental and the numerical results. Section 5 describes the main conclusions drawn by this study.

2. THEORETICAL FRAMEWORK

In the literature on aerosols, the Knudsen number is introduced to schematize the collision and coagulation between particles undergoing Brownian diffusion. Thus, the collision between two spherical particles of radii r and r' is considered in terms of the Knudsen numbers, $Kn = \lambda/r$ and $Kn' = \lambda/r'$ of the two particles, where λ is the mean free path of molecules of the suspending gas. When $Kn \approx Kn' \gg 1$ both particles are in the so-called *free molecular* flow regime and may be regarded as large molecular constituents of a "quasi-Lorentz" gas. In this regime, one has the very accurate expression for the collision coefficient $\beta_c(r, r')$ obtainable from the classical theory of gases. The evaluation of λ at standard temperature and pressure (STP, 273 K, 1 atm) for air molecules and standard density hard spheres is reported for instance by Hinds (48).

In atmospheric flames at about 1500 K the mean free path of gas molecules in the flame is about 350 nm (49). Physically, the motion of the Brownian particle is similar to that of a large molecule that travels in free flight between successive collisions. Unlike the continuum regime, in this case it is possible to calculate directly the number of collisions between the particle and the surrounding gas atoms by statistical mechanics arguments. Thus, the gas and the aerosol particles are in thermodynamic equilibrium and the aerosol velocity distribution is Maxwell–Blotzmann. Collision between particles is assumed to be hard-sphere like; i.e., the cross-section is the geometrical cross-section and it does not depend on particle velocity.

When $Kn \ll 1$ and $Kn' \gg 1$, the particle of radius r is in the *continuum regime* and the collision rate may be obtained very accurately by continuum diffusion theory, wherein the particle of radius r' diffuses as a molecular constitutent to the surface of the large particle of radius r. At the other extreme, when $Kn \approx Kn' \ll 1$ both particles move as Brownian particles in a continuum, where the collision rate expression is also well established. Unfortunately, all other collisional possibilities lie in the intermediate region of Knudsen numbers where no rigorous theory as yet exists. In this regime of intermediate Kn some semitheoretical expressions first derived by Fuchs are available based on the concept of *Fuchs' jump distance* (29, 32, 50, 51). More recently some expressions to estimate the collision rate in the transition regime have been presented by other authors, also in the case of nonspherical aggregates (52, 53), for a review see Seinfeld and Pandis (54).

We start from the evolution equation for the fractal dimension in terms of the number concentration density function. This represents a particular case of the general dynamics equation (GDE) for the case of a coagulation kernel $\beta_c(\cdot)$ depending both on particle volume and fractal dimension. Thus, considering the coagulation process as a collection of two-body interactions between particles with properties (v, D_{f1}) and (v', D_{f2}) the time variation of the number concentration $n(v, D_f, t)$ is written as (47, 55–57).

$$\begin{aligned}\frac{\partial n(v, D_f, t)}{\partial t} = {} & \frac{1}{2}\int_0^v dv' \int_{Df,\min}^{D_{f,\max}} dD_{f1} \int_{Df,\min}^{D_{f,\max}} dD_{f2} \\ & \times \beta_c(v - v', v', D_{f1}, D_{f2}) \\ & \times \delta(D_f - d_f^*(v, v', D_{f1}, D_{f2})) \\ & \times n(v', D_{f1}, t) n(v - v', D_{f2}, t) \\ & - n(v, D_f, t) \int_0^\infty dv' \int_{Df,\min}^{D_{f,\max}} dD_{f1} \\ & \times \beta_c(v, v', D_{f1}, D_f) n(v', D_{f1}, t) \\ & - \frac{\partial \dot{D}_f(D_f, v) n(v, D_f, t)}{\partial D_f} \\ & - \frac{\partial \dot{V}(D_f, v) n(v, D_f, t)}{\partial D_f} + \dot{J}(v^*, D_f, t), \end{aligned} \quad [1]$$

where the symbols are described below.

$n(\cdot)$	Number concentration density function
$\beta_c(\cdot)$	Coagulation rate or collision kernel
v	Particle volume
v^*	Critical volume of nucleii from gas-to-particle conversion
D_f	Particle fractal dimension
$\dot{D}_f(\cdot)$	Rate of fractal dimension variation due to restructuring
$\dot{V}(\cdot)$	Volumetric particle growth rate due to condensation from gas phase
$\delta(\,)$	Dirac delta function
$\dot{J}(\cdot)$	Generalized nucleation rate
t	Time

In the equation above, the term $\beta_c(v, v', D_{f1}, D_{f2})$ represents the *coagulation* (*collision*) *kernel or coefficient* that represents the rate at which aggregates of volume v and v' and fractal

dimension D_{f1} and D_{f2} stick together to form new clusters of volume $v + v'$ and form a new cluster of fractal dimension d_f^*. The term $d_f^*(v, v', D_{f1}, D_{f2})$ provides the fractal dimension of the aggregate resulting from the encounter of two particles with properties (v, D_{f1}) and (v', D_{f2}). A constitutive law for the term $d_f^*(\cdot)$ has been introduced in Kostoglou and Konstandopoulos (47). The term $\dot{J}(v^*, D_f, t)$ represents the rate of nucleation of new particles by nucleation from a gaseous chemical species, which occurs in correspondence of a critical particle size of volume v^*.

The above model stands on the assumptions of negligible evaporation (disconnection) of single primary particles from the clusters and on the fact that all the primary particle/clusters-to-clusters collision are effective (unity sticking coefficient).

A number of approximate situations are possible within the above general framework. Thus, in the case of nearly monodispersed and sufficiently diluted systems undergoing Brownian coagulation in the free molecular regime ($Kn \equiv \ell/r \gg 1$), very often the Smoluchowski equation for sufficiently diluted liquid colloids undergoing coagulation in condition of initial monodisperse population in absence of evaporation and nucleation is reported to apply in the following simple form (55, 58)

$$-dn/dt = \frac{K_c}{2} \cdot n^2, \qquad [2]$$

where $\beta(v, v', D_{f1}, D_{f2})$ now becomes constant and is denoted by K_c (aggregation constant or kernel). In this approach, uncorrelated pair-collisions are considered and the total net rate of particle removal is evaluated on the basis of the total ensemble number of collisions (29). Physically, K_c represents the aggregation rate and depends on size, shape, concentration, and density of the solid particles and temperature, pressure, and viscosity of the surrounding gas.

If K_c is retained constant, then Eq. [2] is written as

$$n/n_0 = 1/(1 + K_c n_0 t/2), \qquad [3]$$

where $\tau_c \equiv (K_c n_0/2)^{-1}$ is the *coagulation time* (time requested to reach the one-half of the initial number concentration n_0 of particles) and $n_0/n(t) = N_P(t)$ is the primary subunits (monomers) per clusters. For free-molecule coagulation in flames of uncharged spherical particles of dimension below 60 nm, Prado and Lahaye (59) obtained

$$\frac{dn}{dt} = -\frac{6}{5}\kappa f_v^{1/6} n^{11/6} \quad \kappa \equiv \frac{5}{12}\left(\frac{3}{4\pi}\right)^{1/6}\left(\frac{6k_BT}{\rho_s}\right)^{1/2} G\alpha, \qquad [4]$$

where f_V, ρ_s are the particle volume fraction and particle density and k_B is the Boltzmann constant. G is a factor which accounts for the interparticle dispersion forces (valued to be about 2 for spherical particles), and α is a weak function of the particle size distribution, reflecting the variation in collision efficiency with different particle sizes.

The above formulation corresponds to the former results derived by Lai *et al.* (26) who showed that the coagulation process of a self-preserving aerosol population in the free molecular regime can be described by (60)

$$\frac{dn}{dt} = -\frac{\alpha_1}{2}\left(\frac{3}{4\pi}\right)^{1/6}\left(\frac{6k_BT}{\rho_S}\right)^{1/2} f_v^{1/6} n^{11/6}, \qquad [5]$$

where $\alpha_1 = 6.67$. In the above, as recognized by McMurry and Friedlander (61), the constant α_1 should depend on both the rate and the specific mechanism of gas-to-particle conversion, which influence the shape of the self-preserving distribution.

Integrating at constant fv and T, for large values of $n_0 (n_0 > 10^{18}$ part/m^3) the solution is

$$n \propto \left[T^{1/2} f_V^{1/6} t\right]^{-6/5}. \qquad [6]$$

In the case of free molecular or Epstein Regime, namely, $Kn \equiv \ell/r \gg 1$, the coagulation kernel can be written as (28)

$$\beta_c(v, v') = \left(\frac{3}{4\pi}\right)^{\frac{1}{6}}\left(\frac{6k_BT}{\rho_P}\right)^{\frac{1}{2}}\left(v^{\frac{1}{3}} + v'^{\frac{1}{3}}\right)^2\left(\frac{1}{v} + \frac{1}{v'}\right)^{\frac{1}{2}}, \qquad [7]$$

where ρ_P is the density of the individual sphere. In the case of monodisperse coagulation $v = v'$, Eq. [7] reduces to

$$\beta_c(v) = 2^{5/2}\left(\frac{3}{4\pi}\right)^{1/6}\left(\frac{6k_BT}{\rho_P}\right)^{1/6} v^{1/6}. \qquad [8]$$

Equation [8] written above is derived from the kinetic theory of gases for collision between molecules which behave as rigid spheres noninteracting between them with a characteristic dimension that is small compared to the mean free path λ of the carrier gas. The term "noninteracting" as reported by Lai *et al.* (26) indicates (quoting those authors) that "no forces of interaction like electrical forces or intermolecular forces are significant in the collision process. The particles are assumed to stick together with unit probability when their surfaces touch."

When the sticking coefficient is introduced in the theoretical scheme, Eq. [7] is written as the following equation for the rarefied gases which describes each primary particle as a large molecule undergoing independent binary collisions with the gas molecules

$$\beta_M(R_1, R_2) = \alpha\pi(R_1 + R_2)^2\left(c_1^2 + c_2^2\right)^{1/2}, \qquad [9]$$

where R_1 and R_2 are the radii of the approaching particles, α is the sticking probability (it is considered 1 in previous Eq. [7]), and $c_i = [(8k_BT)/(\pi m_i)]^{1/2}$ is the root mean square velocity for a particle with mass m_i (48).

With primary particle density equal to $\rho_P = 2000$ kg/m^3 (62), β_c is $3.8717 \times 10^{-11} \cdot v^{1/6}$ (SI) at $T = 1823$ K. For $D_P = 5 \times 10^{-9}$ m, 10×10^{-9} m, 20×10^{-9} m, 30×10^{-9} m, 40×10^{-9} m, β_c is 2.45×10^{-15} m^3/s, 3.47×10^{-15} m^3/s, 4.92×10^{-15} m^3/s,

6.02×10^{-15} m^3/s, and 6.95×10^{-15} m^3/s that are, respectively, values considerably larger than the coagulation constant reported in the continuum regime ($D_P > 100$ nm, $D_P > \lambda_P$) by Hinds (48). The Hamaker constant can be eventually introduced to represent the enhancement in the collision rate by the van der Waals forces (29).

In the mathematical sense Eq. [8] represents a homogeneous function of order 1/6 in particle volume (63). Lai *et al.* (8) and Friedlander (5) consider a similarity transformation to derive a solution of the GDE equation in absence of both particle nucleation, $\dot{J}(v^*, D_f, t) = 0$, and growth, $\dot{V}(v) = 0$. The change in the total number of particle with time is found to be

$$\frac{dn_\infty}{dt} = -\frac{\alpha}{2}\left(\frac{3}{4\pi}\right)^{1/6}\left(\frac{6k_BT}{\rho_P}\right)^{1/2} V^{1/6} n_\infty^{11/6}, \qquad [10]$$

where $\bar{v} = V/n_\infty$ is the average particle volume, n_∞ is the total number of particles for unit volume of fluids $n_\infty = \int_0^\infty n\, dv$, and V is the total volume of particles for unit volume of fluid $V = \int_0^\infty n\, v\, dv$ or in the case of monodispersion $V = \pi n_\infty D_P^3/6$.

The continuum or Stokes–Einstein regime is obtained for $Kn \equiv \ell/r \ll 1$ namely in the case that the particle is large compared to the mean free path. If the Stokes–Einstein expression for the diffusivity coefficients is assumed to be valid, then the Smoluckowski continuum coagulation coefficient (collision parameter) can be written as (29)

$$\beta_c(v, v') = \frac{2k_BT}{3\eta}\left(v^{\frac{1}{3}} + v'^{\frac{1}{3}}\right)\left(\frac{1}{v^{1/3}} + \frac{1}{v'^{1/3}}\right), \qquad [11]$$

which is very different from Eq. [8] in that here η is the gas viscosity, namely a property of the gas and not of the solid sphere. Physically, the fluid is trapped in the agglomerate and the whole system (solid plus gas) moves as if it were a compact sphere of radius of gyration R_g. The flight of the Brownian particle is therefore described by the Langevin equation with an appropriate noise source term which accounts for the molecular impact (29). It is significant to emphasize that the decay law shown previously for particle number concentration in the free molecular regime $dn_\infty/dt \propto n_\infty^{11/6}$ is different from the corresponding law in the continuum range for which dn_∞/dt is proportional to n_∞^2.

For mass fractals, the equation between mass M, radius of gyration of the cluster R_g, size of primary particles D_P, and fractal dimension D_f is written as

$$M \propto (2R_g/D_P)^{D_f}. \qquad [12]$$

Based on the proportionality of mass and volume of the cluster through the cluster density, the following relationship between the radius of gyration R_g and the volume v of the cluster can be easily derived:

$$R_g \propto v^{1/D_f}. \qquad [13]$$

Substituting the above in the expression for the coagulation coefficient it is possible to obtain the expressions for the coagulation coefficient in the two cases of free molecular limit and continuum limit as reported in detail by previous authors (10, 28).

3. EXPERIMENTAL FINDINGS

A diffusion flame is obtained by fueling a Bunsen burner with inner diameter 10 mm with bottled ethylene. The flame is characterized by an apparent length of 170 mm corresponding to a cold-gas velocity out of the burner exit $v_{\text{cold-gas}} = 14.5$ cm/s. To provide repeatability of measurement, the air inlet at the base of the Bunsen burner is blocked in a reference position that produces a fuel rich and very sooting flame.

A noninvasive experimental method to determine *in situ* the absolute size of soot primary particles generated in such kind of flame, which is based on the fast fourier transform (FFT) inversion of the structure function experimentally determined by light scattering angular pattern, has been reported and widely discussed elsewhere (46). The average primary particle size of soot agglomerates growing along the central portion of a diffusion flame is obtained with thermophoretic sampling on a quartz support and analysis using a field emission gun scanning electron microscope (SEM, LEICA Cambridge Ltd., Stereoscan 360 FE).

Different samples have been taken at different heights-above-burner within the flame at radial coordinate zero, corresponding to the same locations of the probing volume *MV* determined in the light scattering experiments. Samples from flame are lodged inside a rotative pump (Xenosput model XE 200) with vacuum at 10 μm Hg and are subjected to a metalization process. This consists in the deposition of a chromium coating film of 1.5 nm thickness, typically, on the sample surface. The magnification of SEM images, printed on Polaroid supports, is typically 60,000 to 120,000 times for an acceleration voltage of about 15.0–25.0 kV. SEM images are inspected directly in the central zone of the sample and about 50 particles are sized to evaluate the average primary particle dimension. Attention is given to the collection of samples with sufficiently low surface concentration of particles to avoid partial aggregate overlapping.

The experimental set-up for light scattering measurements is detailed in previous work (46, 62). The measurement volume *MV* is positioned along the flame axis at different heights z. *MV* is about 40.7×10^{-6} mm^3 at 90°, corresponding to a half-angle of detection equal to 3.2°. The first appearance of soot (transition from a bluish to a yellow flame) is observed at the $z_{\min} = 2$ mm, where soot particles come into existence. Gas temperature is measured according to a rapid insertion procedure commonly used in the literature (64–66). In particular, in correspondence to the same locations on the flame centerline where light scattering measurement volume lies, we insert very quickly (to avoid damage) an uncoated thermocouple Pt–Pt 13% Rh with a bare junction of 25 μm in diameter. The thermocouple support is mounted on a translation stage so that the junction can be

moved back and forth thus being positioned at the measurement location (near the centerline of the flame) and quickly retracted outside the flame. The insertion time of the uncoated junction at the measurement location is about 300 ms. Measured peak temperature obtained as an average of 50 measurements was about $T_c \approx 1700 \pm 80^\circ$K at 30 mm above the burner at radial coordinate zero, respectively. The cooling rate of the bare junction immediately after the junction retraction outside the flame is on the order of 200 K s^{-1}.

The peak temperature values are then corrected for radiative loss from the bead (junction) of the thermocouple using the method described by Fristrom and Westenberg (67) by equating the heat transferred to the probe from the gas to that lost by radiation. In our case the thermocouple junction is a nearly perfect sphere of typical diameter less than about 150 μm as observed under a microscope (Nikon, SMZ-1). Not visible deposition of soot on thermocouple is detected and therefore the bead emissivity is taken to be that of bright Platinum at about 1700 K, namely $\varepsilon = 0.25$ (68). Following this procedure the maximum correction applied to the temperature data is approximately 90 K. After each measurement series the thermocouple junction bead is carefully passed within the bluish soot-free flame zone to eliminate soot and impurities eventually deposited on it.

Therefore, the gas temperature is evaluated along the flame centerline at $\mathbf{z} = 20$ mm as $T_g \approx 1800 \pm 80$ K, taking into account the correction for radiation loss (67). The gas temperature is about 300 K at the burner exit. Thus, the conversion from height to residence time is performed by the equation $(z - z_{\min}) = v_{\text{cold-gas}} \cdot (1800/300) \cdot t$. This is expected to introduce an error on the particle velocity, especially at higher heights above the burner. Thus, we limit our measurements to heights smaller than one fourth of the flame apparent height. The laser light source is an Argon Ion Laser ($Ar+$), operating at line 514.5 nm with output power 350 mW. The polarization state of the laser light is linear vertical. The laser light is modulated on–off by a programmable chopper at 931 Hz. The scattered light is collected at angles θ between 10° and 160° by a rotating optical system composed of an interference filter (half-width spectral response 1.043 nm), two plane-convex lenses (focal lengths 300 and 50 mm), a pinhole (diameter 1 mm), a polarizing beam splitter (PBS) cube, and two *side-on* photomultiplier tubes. A lock-in amplifier operating on the chopper frequency is used to discriminate light scattering signals from flame luminosity and to reject out-of-band noise. Thus, the scattered light is split by the PBS into one contribution with the same linear polarization state of the incident light, written as I_{VV}, and one other with polarization orthogonal with respect to the incident light, I_{HV}. Thirty-eight measurements at different polar angles in the range 15° to 160° are taken in a single experiment. In terms of the modulus q of the wave vector, this corresponds to the range $2.0\ \mu\text{m}^{-1} < q < 24\ \mu\text{m}^{-1}$. Angular patterns of scattered light are measured at heights above the burner (HABs) between 4 and 36 mm at radial coordinate zero (along the flame axis).

The standard procedure to obtain the morphological parameters of the aggregates by the reduction of the experimental data is reported elsewhere (46). In Table 1, we show four examples of determination of fractal dimension D_f, radius of gyration R_g from scattering measurements, and of primary particle size D_P obtained by SEM analysis of samples taken in correspondence to the location of MV within the flame by thermophoretic probing. The experimental uncertainty in the primary size determination is on the order of 15% owing to the fact that partial coalescence of primary particles typically occurs with the formation of neck-like contacts between single particles.

TABLE 1

Examples of Fractal Dimension, Radius of Gyration, and Mean Primary Particle Size as Determined from Experiments at Different Residence Times at the Central Location within the Diffusion Flame

HAB (mm)	t (ms)	D_f	R_g (nm)	$D_{P,\text{SEM}}$ (nm)
10	9.2	1.25	232	22
16	16.1	1.22 ± 0.10	380 ± 24	32 ± 5
26	27.6	1.46	159	38
36	39.1	1.9	267	45

Note. Columns 1 and 2 show the heights above the burner and the residence times at the central location (zero radial coordinate within the flame). Same experimental conditions as in Figs. 1–5. Columns 3 and 4 report the values of fractal dimension and radius of gyration inferred from the measurements of the angular patterns of the scattered light intensity I_{VV}, according to the procedure detailed in previous work (46, 62). The mean primary particle dimensions as obtained from SEM analysis are shown in column 5. The experimental uncertainties in measurements of D_f, R_g, and $D_{P,\text{SEM}}$ are about 8, 7, and 15%, respectively.

Figure 1 shown residence times vs the fractal dimension D_F and the gyration radius R_g obtained by the angular patterns of I_{VV} at different residence times t. We observe that the behavior of D_F is in accordance with the results reported by Mikhailov and Vlasenko (69). Thus, the aggregation process normally starts as cluster–particle interaction. The fractal dimension is typically decreasing and it tends to be about 1.2 at about 10 ms, which is characteristic of chain-like clusters, by the effect of the formation of primary clusters with strong anisotropy. At this stage, charge effects on aggregate surfaces related to the different local hydrogen contents can probably justify the effect of charge migration on the aggregate surface when the sticking of new spherules to the aggregate induce the formation of contact potential on the cluster surface. The net effect of such a charge mechanism can favor the formation of clusters with a low fractal dimension (37). At later residence times (above ~40 ms) the cluster–particle interaction produces a gradual decrease in growth anisotropy and more compact fractal clusters with fractal dimension of about 1.9 are obtained. This experimental result is very close to the value $D_f = 1.8$, which is usually reported in the literature from the numerical simulations in the case of a diffusion-limited cluster–cluster aggregation process (70).

It is significant to stress that the basic requirement for a correct assessment of the fractal dimension is that the ratio between the radius of gyration and the primary radius is larger than about 10 (7). Stated in other words, the fractal analysis is justified only for the scattering from bigger aggregates on scales which

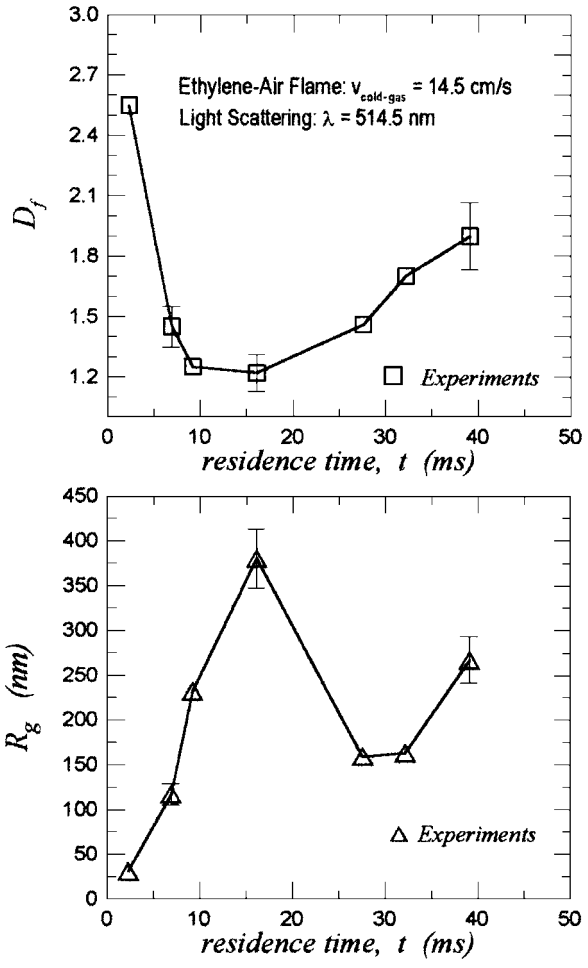

FIG. 1. Fractal dimension (at top) and radius of gyration (at bottom) vs residence times as inferred from vertical–vertical scattered light intensity measured in the ethylene–air flame at radial coordinate zero (flame axis). Cold-gas velocity is $v_{\text{cold-gas}} = 14.5$ cm/s. Times are estimated by the equation $(z - z_{\min}) = v_{\text{cold-gas}} \cdot (1800/300) \cdot t$, where $z_{\min} = 2$ mm is the minimum quote where soot comes into existence.

considerably exceed the size of the primary particles. Smaller soot agglomerates do not respect strictly the self-similarity requirement but they obey a relation of the type $M \propto (2R_g/D_P)^{D_f}$ (this is reflected in the term *fractal-like* or *power-law* agglomerates). Thus, the parameter D_f can be determined also for agglomerates composed of some tens of particles. This is significant in making a quantitative assessment of the capacity by the clusters to fill the space that they occupy.

It should be noted that at residence time $t \approx 30$ ms a minimum of measured fractal dimension is observed in correspondence to the condition of maximum radius of gyration. After $t \approx 30$ ms the agglomerates tend to reshape into more compact clusters (increasing fractal dimension), and the radius of gyration diminishes correspondingly. At about 40 ms, when more structured fractal units of about 260 nm radius of gyration are formed, a new regime of clustering of super-primary particles starts, as confirmed by the diminishing of the measured dissymmetry ratio $R_{VV}(20^\circ/90^\circ)$, shown in Fig. 2 at different residence times for the same flame conditions of Fig. 1. It should be stressed that $R_{VV}(20^\circ/90^\circ)$, that is the ratio $I_{VV}(20^\circ)$ to $I_{VV}(90^\circ)$, is expected from computations to increase monotonically with respect to the addition of new monomers to the cluster (71), namely with respect to the mean number of primary particles per cluster N_P. This result holds true whatever the cluster morphology for such dissymmetry ratio but not for other $R_{VV}(\theta_1/\theta_2)$ as verified from numerical computations (71). Thus, typically, the predicted values of $R_{VV}(20^\circ/90^\circ)$ for chain-like aggregates are much *higher* than those evaluated for fractal cluster at parity of the number of spherules in the cluster. Comparative work between measurements and predictions was performed to correspond at different residence times the measured values of primary particle size by SEM analysis, the radius of gyration and fractal dimension, and the $R_{VV}(20^\circ/90^\circ)$ obtained by the light scattering experiments.

Following this procedure by trial and error in the unknown N_P it is possible to recognize that in the region of the flame center corresponding to z between about 8 and 16 mm (residence times from about 7 to 16 ms) chain-like structures do form with a number of primary particles per cluster starting from about 10 to about 50 units for increasing t. This mechanism is observed due to the monotonical increase of the measured $R_{VV}(20^\circ/90^\circ)$ that starts at $t < 7$ from unity, which is the value for isolated Rayleigh spherules, to about 8 ($t \approx 16$ ms), corresponding to the joining of fresh primary particles to the chain tips. The origin of the entropically favorable sticking by the primary particles at the chain tips is probably electrical in nature as discussed in detail elsewhere (37). These "primary" chains represent, on their own,

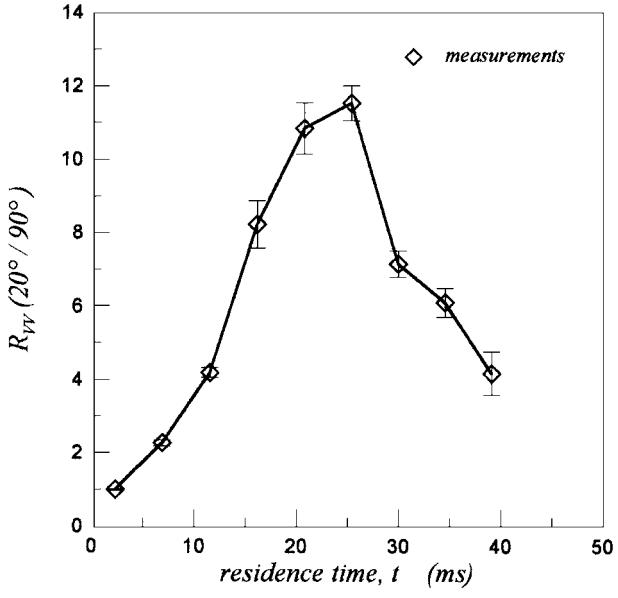

FIG. 2. Dissymmetry ratio $R_{VV}(20^\circ/90^\circ)$ vs residence times the light scattered with the same linear vertical polarization of the incident light. $R_{VV}(20^\circ/90^\circ)$ indicates the ratio of the measured $I_{VV}(20^\circ)$ to $I_{VV}(90^\circ)$, respectively. Ethylene flame is the same as described in Fig. 1.

"macro" soot parcels that, thereafter, for z above 16 mm and below about 28 mm (residence time in the range 16 to 30 ms), undergo agglomeration and form more complex structures corresponding to chain arrays formed by multiple adjacent rows. The "macro" chains formed in correspondence with $z \approx 16$ mm are of considerable dimension (radius of gyration up to about 380 nm), being constituted by a number of primary particles estimated at about 100. At this stage the maximum measured value of the dissymmetry ratio $R_{VV}(20^\circ/90^\circ)$ is about 11. At residence times above about 25 ms, the collapsing of these chain-like elongated structures is observed with the clustering of such "macro chains" in complex fractal assemblies with D_F in the range 1.5 to 1.9. The $R_{VV}(20^\circ/90^\circ)$ measured at this stage is considerably lower with respect to the elongated chains observed at smaller residence times. In particular, it decreases from 11 to about 4 for residence times from about 25 to 40 ms. It should be stressed that the dissymmetry ratio technique is a very powerful technique, which is weakly depending (71) on the soot refractive index, a property that is recognized to vary considerably at different residence times.

The measurements of the depolarization ratio $\rho_V(90^\circ)$, reported in previous work (62), are also compared with the other measured quantities in order to recover the qualitative feature that chain-like elongated clusters produce a larger depolarization, owing to their more pronounced anisotropy with respect to more compact morphologies. In fact, ρ_V should be zero for homogeneous spherical structures independent of size. Thus, the measurements show that $\rho_V(90^\circ)$ monotonically increases for HABs between 8 and 20 mm (t between about 7 and 25 ms), which corresponds to the mechanism of long chain formation with pronounced anisotropy, which was previously observed from the independent measurements of $R_{VV}(20^\circ/90^\circ)$. For residence times longer than about 25 ms, the measured $\rho_V(90^\circ)$ is lower and corresponds to the formation of fractal structures with higher fractal dimension and overall smaller anisotropy.

Following the procedure detailed above, we report in Fig. 3 (circles) the mean number N_P of primary particles per aggregate against the residence time. We question at this point the possible choice of the coagulation kernel. It is believed that the linear shape of the initial aggregates implies that the new contacts are formed by the primary particles located at the edge of the aggregate. The most probable reason for this growth pattern is the existence of strong repulsive forces between the aggregates. These forces cause the aggregates to find the configuration which minimize the repulsive force barrier, i.e., the configuration of aggregation in linear chains. The origin of the repulsive forces between particles could be electrical in nature, as discussed above. For this mode of aggregation it is found from the experiments that the coagulation rate is *almost independent* of the aggregate size. This result can be explained from the fact that the cross section area for the coagulation is not the entire aggregate surface but instead the surface of the primary particle lying on the boundary of colliding aggregates. Therefore, the assumption of a constant kernel for the coagulation process is compatible with the experimental evolution of the N_P. The initial (at time indicated in the following as t_0) size and concentration of primary particles $D_P = 6\,\text{nm}, n_0 = 3.0 \times 10^{12}\ \text{cm}^{-3}$ are inferred from SEM analysis and extinction measurements, respectively, corresponding to the strong increase of both depolarization ratio $\rho_V(90^\circ)$ and dissymmetry ratio $R_{VV}(20^\circ/90^\circ)$ at about 2.5 ms ($z = 4$ mm), see Fig. 2. The best fitting of the analytical equation $N_P = 1 + \beta_c n_0 (t - t_0)/2$ to the experimental data of N_P yields $\beta_{c,\text{exp}} \approx 2.37 \times 10^{-9}\ \text{cm}^3/\text{s}$, squared regression coefficient $R^2 = 0.993$, a traslation $t_0 = 1.43$ ms, and $\tau_{c,\text{exp}} \approx 0.28$ ms, from the relationship $\tau_{c,\text{exp}}/\tau_{c,\text{th}} = \beta_{c,\text{th}}/\beta_{c,\text{exp}}$. On the other hand, being that the coagulation kernel (48) is a function of size and concentration of primary particle nuclei and of temperature, namely $\beta_{c,\text{th}} = \beta_{c,\text{th}}(D_P, n_0, T)$, the theory of coagulation in free molecular regime (23, 48) allows to predict (Eq. [8] with sticking probability $\alpha \approx 1$, $D_P = 6$ nm, $n_0 = 3.0 \times 10^{12}$ part/cm^3)$\beta_{c,\text{th}} \approx 2.69 \times 10^{-9}\ \text{cm}^3/\text{s}$ and $\tau_{c,\text{th}} \approx 0.25$ ms.

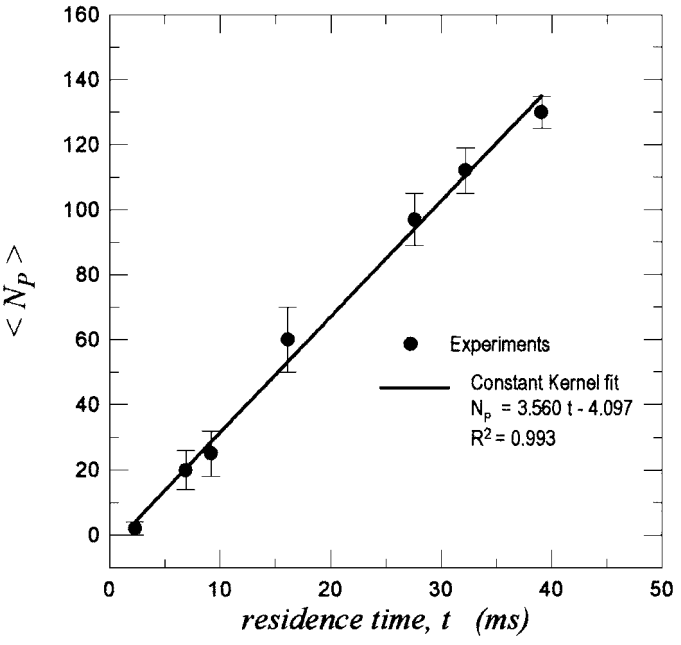

FIG. 3. Mean number N_P of primary particles per aggregate vs residence time as inferred by the measurements of I_{VV} that yields D_f, R_g, and of $R_{VV}(20^\circ/90^\circ)$. Primary particle size D_P is obtained from SEM analysis of soot samples (same flame of Fig. 1).

As a comment about the experimental results with respect to the corresponding predictions in the free molecular regime in the case of smaller particles $5 < D_P < 10$ nm, it should be stressed that the expression of the collision coefficient obtained from the kinetic theory of rarefied gas does contain a phenomenological sticking probability term and is written in the general case as (Eq. [8] is here rewritten in the case of identical primary particles) $\beta_M = \alpha\sqrt{2}\pi D_P^2[(8k_BT)/(\pi m_P)]^{1/2}$. Following Fuchs and Sutugin (32), taking into account the interparticle forces and assuming a Hamaker constant $A \approx 10^{-19}$ J it is possible to compute (31) the constant enhancement factor y in the collision

cross-section as $y \approx 1.7$ for primary particles of about 5 nm. Thus, the computed collision rate $\beta_{c,\mathrm{th}} \approx 2.69 \times 10^{-9}$ cm^3/s should be corrected for the smaller particles ($50 < Kn < 70$, $\lambda \approx 350$) by multiplication times the enhancement factor y. Nevertheless, it is recognized that the sticking probability, defined as the ratio of the number of captures and the number of collisions between particles undergoing agglomeration, is vanishingly small for particles of very small size and reaches an asymptotic value 1 for larger particles. At a gas temperature of about 1800 K, such as in our case, corresponding to a Hamaker constant $A \approx 10^{-19}$ J and interparticle interactions described in terms of the Lennard–Jones 6–12 potential, the sticking coefficient can be retained as unity for particles larger than about 10 nm, even though for smaller primary particle sizes it can be less than unity. Also, the predictions obtained by other authors from Monte Carlo simulations (72) that take into account the van der Waals attraction and the Born repulsion between particles instead of the approach of sticking probability predict a collision efficiency, defined as the ratio of the number of captures to the number of collisions between particles undergoing agglomeration, that is, smaller than unity for particles of very small size. For instance, the same authors (73) furnish the prediction for the ratio γ between the coagulation coefficient from simulations and the Smoluchowski coagulation coefficient for equal size spheres as $\gamma = 0.12, 0.50, 0.75$ in the case of particles with unity density and dimensions $D_P = 5, 10, 15$ nm ($\lambda = 350$ nm, $Kn = 70, 35, 23$, respectively) at 1 atm, 298 K, and with a Hamaker constant $A = 10^{-19}$ J. Thus, for smaller particles, it could happen that the eventual increase in the rate of collision is counterbalanced by the decrease in the effectiveness of the same collisions.

In conclusion, for the smaller soot nanoparticles investigated here ($5 < D_P < 10$ nm), the net effect of an increase of collision rate as opposed to a sticking efficiency slightly less than unity, is, probably, that the coagulation coefficient remains at about the same value at different residence times. This can be interpreted at the later stage of the agglomeration process (larger primary particles, about 10 nm) as a lower rate of collisions between particles themselves with a high collision efficiency α (about unity), with respect to an enhanced rate of collisions with a smaller α corresponding to the early stage of the process (smaller primary particles, about 5 nm).

In Fig. 4, the mean number of cluster concentration n_A vs residence time is evaluated as the ratio between the primary particle concentration n_0 and $N_P(t)$. In this regard, residence times longer than about 1.43 ms (height-above-burner over 10 mm) are considered. In such cases, the nucleation phase, namely the process of generation of fresh nuclei of soot particles can be considered complete as observed by the scarce surface growth found from SEM analysis. As a consequence of this, the number concentration n_0 of the primary particles remains essentially constant after 1.43 ms and equal to 3.0×10^{12} cm^{-3} as inferred by extinction measurements. In particular, coherently with the conclusions drawn from Fig. 3, corresponding to residence times above 10 ms (HAB > 10 mm) a *cluster–cluster* agglomeration

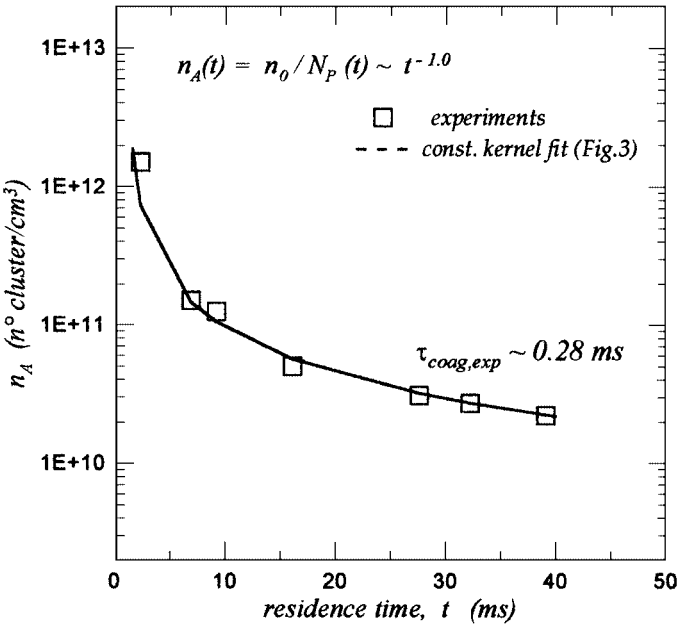

FIG. 4. Mean number of cluster concentration vs residence time (same flame of Fig. 1).

regime is found to occur with an observed coagulation time constant $\tau_{c,\mathrm{exp}} = 0.28$ ms corresponding to a constant coagulation kernel. A weak surface growth still is observed at this stage by the measurement of primary size against t (see following Section 4). At later stage of coagulation, chain-like aggregates collapse into more compact structures. In any event, the observed coagulation time constant remains $\tau_{c,\mathrm{exp}} \approx 0.3$ ms during the entire time window of observation.

Figure 5 shows (empty square points), in a double logarithmic scale, the soot volume fraction f_V vs the residence time t as inferred from the measurements of primary particle size D_P from the SEM analysis and the values of the cluster number concentration n_A as obtained from light scattering experiments. The volume fraction is found to increase from about 10^{-6} to about 10^{-4} during the process of aggregate formation.

From a chemical point of view, it is interesting to consider (74) the so-called growth rates per unit surface area or *specific surface growth rates* written as

$$(1/S_u)\, dM_u/dt, \qquad [14]$$

where M_u is the total soot mass in the unit volume in g/cm^3 and S_u is the soot surface area per unit volume $S_u = n_A N_P \langle D_P^2 \rangle \pi/4$.

The values of the specific surface growth rate are shown in Fig. 6. M_u is evaluated converting the experimental data on $f_V(t)$ via the primary particle density as the product $M_u = \rho_P f_V$, where ρ_P is 2.0 g/cm^3 as measured by helium pycnometry experiments (62). The time derivative of M_u is approximated by the finite difference representation. In the previous equation the brackets $\langle\rangle$ indicate the number average, namely the

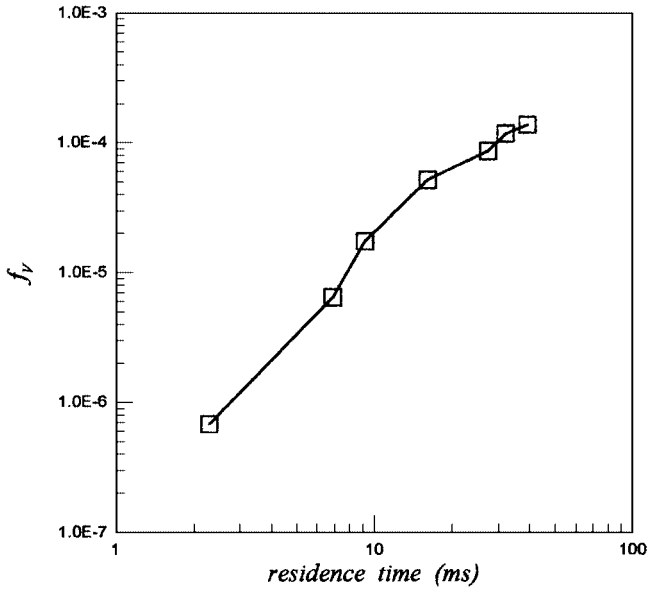

FIG. 5. Soot volume fraction at different residence times (same flame of Fig. 1). Symbols represent the values from experiments (D_P from SEM, N_P, and n_A from Figs. 3 and 4). Solid line is obtained by joining each pair of experimental points with a straight line.

average with respect to the size distribution of particles that is expected to be self-preserving for free molecule coagulation (75). The above evaluation of S_u is valid in the case that primary spheres are smooth; i.e., no pores or cavities are presented on their surface. Both M_u and S_u are functions of the residence time via the primary particle size. The specific surface rates are directly linked via the rate constant k to the heterogeneous reaction which describes the the gas-to-solid conversion. For instance, in the case of acetylene the equation is written as $(1/S_u)dM_u/dt = k[C_2H_2]^j$, where j is the order of the reaction with respect to C_2H_2 (76). The range of values of the specific surface growth rates found here are in accord with the typical data reported in the previous literature (77).

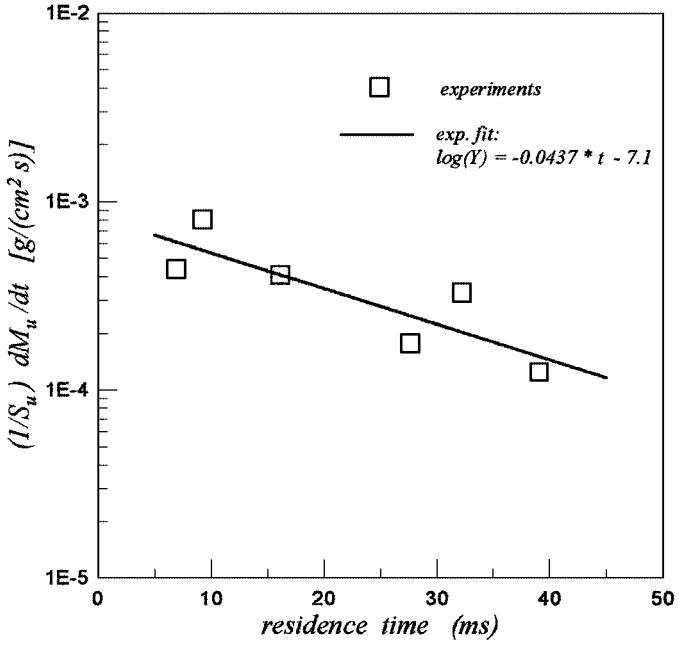

FIG. 6. Apparent specific surface growth rate from the experimental data as a function of the age of the soot particles.

4. NUMERICAL SIMULATIONS OF PRIMARY GROWTH AND FRACTAL AGGREGATE HISTORY

As a general consideration all the rate functions introduced in Eq. [1] are unknown and they must be found (in principle) from the experimental measurements of the aggregate evolution (this is the so-called inverse problem). But even the direct solution of the above equation is very difficult while the solution of the inverse problem is presently intractable. In this work, we adopt the approach of decomposing the inverse problem to smaller subproblems for each process separately by thorough accounting of the experimental data. For example, by observing the total number of primary particles that is constant one can conclude that the nucleation already has been completed before the manifestation of the other phenomena. This is already a major simplification. The three processes in which the problem is decomposed here are: the growth by the vapor phase, the aggregate coagulation, and the evolution of the aggregate morphology as described within the limits of the fractal dimension.

As much as the growth mechanism of primary particles is concerned, the main assumption here is that the coagulation process does not influence the growth process. The primary particles retain their identity in the aggregate and they are all assumed to grow at the same rate as if isolated. The reduction of the growth rate as the time proceeds (see Fig. 7 below) is not an effect of coagulation but it is due to the reduction of the condensible species concentration which in turn is due to the particle growth.

The shape of primary particles is assumed to be spherical. This shape must be retained in the aggregate even if the shadowing effect from the aggregate leads to nonuniform local growth rates, in order that the surface energy be minimized. The prevailing mechanism of the particle growth under the present experimental conditions is the molecular bombardment from the gas phase (23).

The equation for the evolution of the primary particle diameter in free molecular regime can be calculated from kinetic theory (23, 48, 54) and it is written as

$$\frac{dD_P}{dt} = 2v_m\alpha(p_i - p_{i,d})/\sqrt{2\pi mkT}, \qquad [15]$$

where α is a correction factor due to noncontinuum effects and imperfect surface accommodation (usually α is set to unity), v_m is the molecular volume of the condensing i-species, p_i is the vapor pressure far from the particle, $p_{i,d}$ is equilibrium vapor

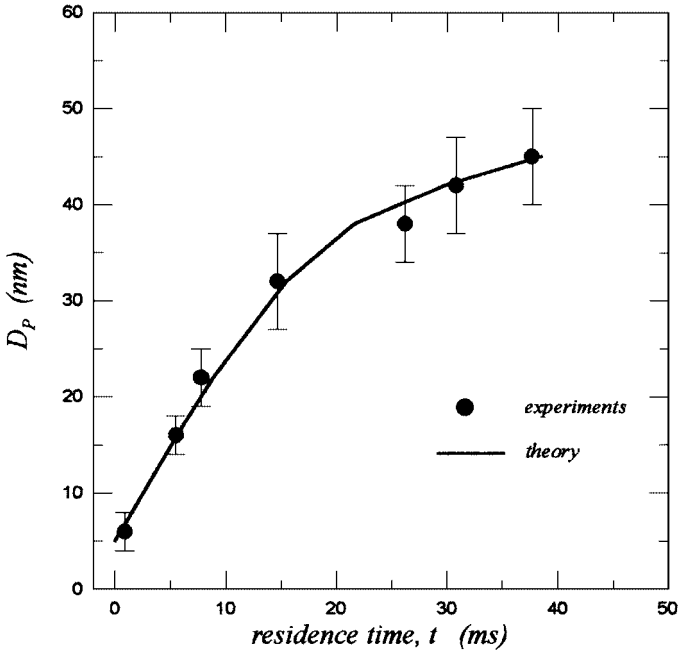

FIG. 7. Comparison between primary size from measurements (SEM) and numerical simulations of primary growth. Size of primary particles is inferred by SEM analysis as average value over a number of 50 measurements from samples taken on the flame axis at different heights above the burner.

pressure just above the surface of the particle (drop) of diameter D_P, m is the mass of the condensing i-molecule flowing to the surface of the particle.

Although the functional form of the growth rate is known, numerical evaluations are not possible due in principle to the unknown molecular volume v_m of the "soot forming species" and its accommodation coefficient α or molecule-particle sticking efficiency (23). In addition, the aggregate shadow effect may change the growth rate. In the following a general model is developed to describe primary particle growth in the free molecule regime from a generic "soot forming species" and then it is fitted to the experimental results to find the parameter values.

We will rewrite the above Eq. [15] as the following equation for volume fraction time-evolution

$$\frac{dD_P}{dt} = 2K_G\varphi, \qquad [16]$$

where K_G is the growth rate constant (nm/s) and ϕ is a driving force factor (dimensionless) for particle growth which is equal to the difference between the actual volume fraction of condensable species i in the gas and the equilibrium one, multiplied by the ratio of gas density to condensate density. Therefore,

$$\varphi = \frac{p_1 - p_d}{P}\frac{\rho_a}{\rho_s}, \qquad [17]$$

$$K_G = \frac{v_m P}{(2\pi mkT)^{0.5}}\frac{\rho_s}{\rho_a}, \qquad [18]$$

where ρ_a is the density of the condensable species in the gas phase, ρ_s is the density of the condensate, respectively, and P is the background pressure.

The conservation equation for mass (density ρ_P) is then expressed as the following equation for particle growth evolution

$$\frac{d\varphi}{dt} = -\frac{\pi}{2}N_p n_0^2\frac{dD_P}{dt}, \qquad [19]$$

where n_0 is the number concentration of the primary particles at the beginning of the coagulation process. Equation [19] is integrated with respect to t and φ is substituted from Eq. [16] thus yielding

$$\frac{dD_P}{dt} = 2K_G\left(\varphi_o + \frac{\pi}{6}n_0 D_{P,0}^3 - \frac{\pi}{6}n_0 D_P^3\right), \qquad [20]$$

where φ_0 is the initial value of the condensible species and $D_{P,0}$ is the initial ($t_0 = 1.43$ ms) diameter of the primary particles. The above differential equation is integrated to give $t = t(D_P)$ as

$$\begin{aligned} t = {} & \frac{1}{6C_1C_2^2}\ln\left(\frac{(D_{P,0}-C_2)^2}{\left(D_{P,0}^2 + D_{P,0}C_2 + C_2^2\right)}\right) \\ & + \frac{1}{3^{0.5}C_1C_2^2}\tan^{-1}\left(\frac{-(2D_{P,0}+C_2)}{3^{0.5}C_2}\right) \\ & - \frac{1}{6C_1C_2^2}\ln\left(\frac{(D_P-C_2)^2}{\left(D_P^2 + D_PC_2 + C_2^2\right)}\right) \\ & - \frac{1}{3^{0.5}C_1C_2^2}\tan^{-1}\left(\frac{-(2D_P+C_2)}{3^{0.5}C_2}\right), \end{aligned} \qquad [21]$$

where $C_1 = \pi n_0 K_G/3$ and $C_2 = (\frac{6\varphi_0}{\pi n_0} + D_{P,0}^3)^{1/3}$.

For the sake of clarity it should be commented that Eq. [21] cannot be solved directly for D_P so a numerical solution is needed to obtain D_P for a particular value of time, thus inverting the relation $t = t(D_P)$ to obtain $D_P = D_P\ (t)$. However, it is much easier to use interpolation from a table of (D_P, t) pairs calculated directly by Eq. [19]. The above model must be fitted to the experimental data in order to find the unknown parameters C_1, C_2, and $D_{P,0}$. The fitting was based on the minimization of the sum of the squares of the difference between the experimental and theoretical values of the diameters. The best fitting parameters were $C_1 = 2.3\text{e-}5$ nm^{-2}/ms, $C_2 = 44.3$ nm and $D_{P,0} = 5$ nm. A comparison between the pairs (D_P, t) obtained via the above calculations and the value of D_P obtained from SEM experiments is reported in Fig. 7.

The point to be stressed is that in the above framework, the values n_0 of the total number of monomers at t_0 and the monomer size D_P are known from the measurements. Therefore, the quantities K_G and φ_0 can be found from C_1 and C_2, respectively, by the best fit to the experimental data. The resulting values

obtained following this procedure are $K_G = 7320$ nm/ms and $\varphi_0 = 1.37 \times 10^{-4}$ and their product (about 1 nm/ms) is in fair agreement both with an estimation of 2 nm/ms for the product $K_G \cdot \varphi_0$ based on a calculation using a density of 2 g/cm^3 for the soot primary particle and assuming that the complete amount of available ethylene generates the "soot forming species" and with the measurements reported previously by other authors (30), who used invasive probing techniques and electron microscopy analysis to probe soot particles in flame.

Simulations have been performed to predict the evolution of the fractal dimension of the aggregates. In Eq. [1] the constitutive law $d_f^*(v, v', D_{f1}, D_{f2})$ should be specified. The form of the constitutive law proposed by Kostoglou and Konstandopoulos (47, 56) is here generalized as

$$d_f^*(v, v', D_{f1}, D_{f2}) = D_{f,\infty} \frac{\ln[2v/\upsilon_P + 2v'/\upsilon_P]}{\ln\left[b(2v/\upsilon_P)^{D_{f,\infty}/D_{f1}} + b(2v'/\upsilon_P)^{D_{f,\infty}/D_{f2}}\right]}, \quad [22]$$

where υ_P is the volume of the primary particles. The parameter $D_{f,\infty}$ is the asymptotic fractal dimension of the system and the parameter b determines how fast $D_{f,\infty}$ is reached by the system, thus the larger (smaller) b representing the faster (slower) approaching of fractal dimension to $D_{f,\infty}$. These two parameters depend on the coagulation mechanism and must be determined in principle from experimental data.

In any case, it is not possible to derive a simple relation between the parameter b and a characteristic time appropriate for this process . This is accomplished only by solving Eq. [1], i.e., by finding the evolution of the fractal dimension.

In the present case for the initial stages of linear aggregates we set the fractal dimension equal to 1 and $b = 1.3$. Based on the data, the coagulation mechanism changes at some time between 15 and 25 ms. We assume that a change in the coagulation mechanism happens at about $t = 20$ ms. The new values of the constitutive law parameters are $D_{f,\infty} = 2.5$ (corresponding to reaction limited aggregation) and $b = 10^4$ (limit of fast fractal dimension evolution). The resulting evolution of the mean fractal dimension of the population using the above approach is shown in Fig. 8. It is very interesting that the theory, which does not account for any restructuring event, cannot predict the large increase of fractal dimension for $t > 20$ ms. This is expected, since the coagulation extent between $t \approx 20$ and $t \approx 40$ ms is not so great as to justify a raise of the fractal dimension from 1.2 to 1.9. In other words it is not possible for coagulation between 60-mers of $D_f = 1.2$ to give $D_{f,\infty} = 1.9$. Vice versa, the restructuring of the aggregates observed in the experiments is responsible for the fast increase of the fractal dimension. Consequently, a restructuring mechanism must be added to the scheme used in the simulations. The simplest model of step-restructuring is described by

$$\frac{dD_f}{dt} = -c(D_f - D_{f,\infty}), \quad [23]$$

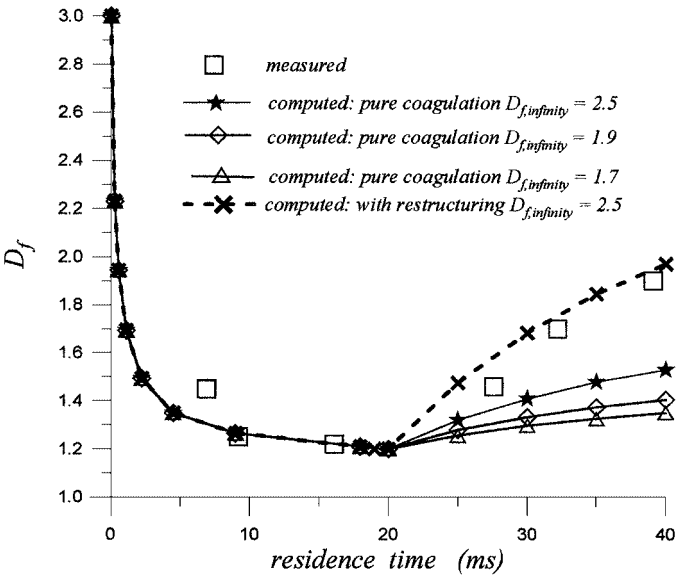

FIG. 8. Comparison between the fractal dimension as measured in the scattering experiments (empty square points) with respect to the numerical simulations implementing solely Brownian coagulation for different asymptotic fractal dimension $D_{f,\infty}$ (continuous curves, $D_{f,\infty} = 1.7, 1.9, 2.5$) or including a step-restructuring process (dashed curve) for $D_{f,\infty} = 2.5$.

where $D_{f,\infty}$ is the asymptotic fractal dimension for the restructured state and the parameter c determines the velocity of approach to the $D_{f,\infty}$. The result of the simulations for $D_{f,\infty} = 2.5$ including the restructuring process with $c = 0.2$ is shown in Fig. 8 as a dotted line with cross symbols and it is compared with the D_f inferred by the scattering experiments. The accord can be considered satisfactory within the experimental uncertainties of both fractal dimension and residence times.

5. SUMMARY

This work has presented the joint results from an experimental and numerical investigation of the kinetics of the agglomeration and growth processes occurring for soot nanoparticles generated in a ethylene–air diffusion flame at atmospheric pressure.

Measurements of fractal dimension D_f and radius of gyration R_g have been performed *in situ* by applying light scattering techniques. Thermophoretic sampling of soot has been used to obtain a standard reference for the size of primary particles at different heights above the burner corresponding to different residence times t. Thus, the mean number of primary particles per aggregate N_P and, accordingly, the aggregate concentration n_A have been inferred at different t.

It has been demonstrated that a constant coagulation kernel provides a good fit of aggregate concentration history. In particular, a coagulation constant $\beta_{c,\exp} = 2.37 \times 10^{-9}$ cm^3/s has been found with a corresponding coagulation time constant $\tau_{c,\exp} \approx 0.28$ ms that is very close to the prediction

obtained for monodispersed aerosols in the free-molecular regime $\tau_{c,\mathrm{th}} \approx 0.25$ ms. This result has been dissused, in the case of the smaller particles ($50 < Kn < 70$, $5 < D_P < 10$ nm), observing that the constant coagulation rate measured in the experiments can be considered as a net constant balance between the effects by two opposite tendencies. These are on one side the finite possibility to escape from a shallow potential well by the very small particles, and, on the other side, the enhancement in the number of particle encounters per second produced as an effect of the relative increase in the range of attraction by the van der Waals force. This mechanism is demonstrated by previous authors (72) to occur on the basis of Monte Carlo simulations of the coagulation process.

Numerical simulations have been performed in order to gain information about the surface growth rate, as obtained from condensation of volatile species onto the surface of the primary particles, and about the evolution of the fractal aggregate morphology, described in terms of the fractal dimension against the residence time. The comparison with the experimental results demonstrates the nice agreement between the primary particle size as measured from SEM experiments and the value computed for particle growth in the free molecular regime with a growth rate constant of primary diameter ∼1 nm/s. The evolution of the fractal dimension as obtained from simulations of the simple agglomeration process without any restructuring is demonstrated to be in adequate to describe the evolution of aggregate morphology evidenced in the experiments. This is thought to be the consequence of a probable mechanism of tempering or graphitization which does occur, for not well understood reasons, by atomic rearrangement in the solid phase carbon as a consequence of the prolonged residence time within the flame. A step-restructuring event is introduced in the numerical code to try to justify the evidence of such an aggregate compacting process. Good agreement is obtained between measurements and simulations when an asymptotic fractal dimension $D_{f,\infty} \approx 2.5$ is considered.

ACKNOWLEDGMENTS

We sincerely thank A. D'Alessio and A. D'Anna from Dipartimento di Ingegneria Chimica of Napoli University "Federico II" for fruitful discussions.

REFERENCES

1. Pratsinis, S. E., *Prog. Energy Combust. Sci.* **24,** 197 (1998).
2. Sorensen, C. M., *Aerosol Sci. Technol.* **35,** 648 (2001).
3. Sorensen, C. M., and Feke, G. D., *Aerosol Sci. Technol.* **25,** 328 (1996).
4. Köylü, Ü. Ö., Xing, Y., and Rosner, D. E., *Langmuir* **11,** 4848 (1995).
5. Dobbins, R. A., and Megaridis, C. M., *Appl. Opt.* **30,** 4747 (1991).
6. Dobbins, R. A., Mulholland, G. W., and Bryner, N. P., *Atmospheric Environ.* **28,** 889 (1994).
7. Martin, J. E., and Hurd, A. J., *J. Appl. Crystallography* **20,** 61 (1987).
8. Bunde, A., and Havlin, S., "Fractals in Science," p. 16. Springer, Berlin, 1994.
9. Bunde, A., and Havlin, S., "Fractals and Disordered Systems," pp. 59–113. Springer, Berlin, 1996.
10. Oh, C., and Sorensen, C. M., *J. Aerosol Sci.* **28,** 937 (1997).
11. Kazakov, A., and Frenklach, M., *Combust. Flame* **114,** 484 (1998).
12. Zachariah, M. R., and Semerjian, H. G., *AIChE J.* **35,** 2003 (1989).
13. Okuyama, K., Kousaka, Y., and Payatakes, A. C., *J. Colloid Interface Sci.* **81,** 21 (1981).
14. Tandon, P., and Rosner, D. E., *Chem. Eng. Comm.* **151,** 147 (1996).
15. Wu, M., and Friedlander, S. K., *J. Colloid Interface Sci.* **159,** 246 (1993).
16. Xing, Y., Köylü, Ü. Ö., and Rosner, D. E., *Combust. Flame* **107,** 85 (1996).
17. Xing, Y., Köylü, Ü. Ö., and Rosner, D. E., *Applied Optics* **38,** 2686 (1999).
18. Appel, J., Bockhorn, H., and Frenklach, M., *Combust. Flame* **121,** 122 (2000).
19. Smoluchowski, M. Z., *Phys. Chem. Abt. A* **92,** 129 (1917).
20. Muller, H., *Kolloid Chem. Beih.* **26,** 257 (1928).
21. Schumann, T. E. W., *Q. J. Roy. Meteor. Soc.* **66,** 195 (1940).
22. Zebel, G. von, *Kolloid Z.* **156,** 102 (1958). [In German]
23. Friedlander, S. K., "Smoke, Dust and Haze—Fundamentals of Aerosol Dynamics." Oxford University Press, New York, 2000.
24. Gillespie, T., *Proc. Roy. Soc. (London) A* **216,** 569 (1953).
25. Rosinski, J., Werle, D., and Nagamoto, C. T., *J. Colloid Sci.* **17,** 703 (1962).
26. Lai, F. S., Friedlander, S. K., Pich, J., and Hidy, G. M., *J. Colloid Interface Sci.* **39,** 395 (1972).
27. Hidy, G. M., *J. Colloid Interface Sci.* **20,** 123 (1965).
28. Mountain, R. D., Mulholland, G. W., and Baum, H., *J. Colloid Interface Sci.* **114,** 67 (1986).
29. Williams, M. M., and Loyalka, S. K., "Aerosol Science Theory and Practice." Pergamon, Oxford, 1991.
30. Wersborg, B. L., Howard, J. B., and Williams, G. C., "XIV Symposium (International) on Combustion," pp. 929–940. The Combustion Institute, Pittsburgh, 1973.
31. Howard, J. B., Wersborg, B. L., and Williams, G. C., "Faraday Symposia of the Chemical Society," no. 7, pp. 109–119. University Press, Aberdeen UK, 1973.
32. Fuchs, N. A., and Sutugin, A. G., *J. Colloid Sci.* **20,** 492 (1965).
33. Okuyama, K., Kousaka, Y., and Hayashi, K., *J. Colloid Interface Sci.* **101,** 98 (1984).
34. Wu, M. K., and Friedlander, S. K., *J. Aerosol Sci.* **24,** 273 (1993).
35. Gorbunov, B., Clarke, A. G., and Hamilton, R. S., *J. Aerosol Sci.* **31,** Suppl. 1, s811 (2000).
36. Weber, A. P., and Friedlander, S. K., *J. Aerosol Sci.* **28,** 179 (1997).
37. Onischuk, A. A., di Stasio, S., Karasev, V. V., Strunin, V. P., Baklanov, A. M., and Panfilov, V. N., *J. Phys. Chem. A* **104,** 10426 (2000).
38. Burtscher, H., and Schmidt-Ott, A., *Phys. Rev. Lett.* **48,** 1734 (1982).
39. Lehtinen, K. E., Windeler, R. S., and Friedlander, S. K., *J. Aerosol Sci.* **27,** 883 (1996).
40. Akhtar, M. K., Lipscomb, G. G., and Pratsinis, S. E., *Aerosol Sci. Technol.* **21,** 82 (1994).
41. Weber, A. P., Baltensperger, U., Gäggeler, H. W., and Schmidt-Ott, A., *J. Aerosol Sci.* **27,** 915 (1996).
42. Julien, R., and Meakin, P., *J. Colloid Interface Sci.* **127,** 265 (1989).
43. Potanin, A. A., *J. Colloid Interface Sci.* **157,** 399 (1993).
44. Martinez-Herrera, J., and Derby, J. J., *AIChE J.* **40,** 1794 (1994).
45. Tandon, P., and Rosner, D. E., *J. Colloid Interface Sci.* **213,** 273 (1999).
46. di Stasio, S., *Appl. Phys. B* **70,** 635 (2000).
47. Kostoglou, M., and Konstandopoulos, A. G., *J. Aerosol Sci.* **32,** 1399 (2001).
48. Hinds, W. C., "Aerosol Technology" 2nd ed. Wiley, New York, 1999.
49. Sorensen, C. M., Cai, J., and Lu, N., *Appl. Opt.* **31,** 6547 (1992).
50. Fuchs, N. A., "The Mechanics of Aerosols." Pergamon Press, New York, 1964.
51. Middleton, P., and Brock, J., *J. Colloid Interface Sci.* **54,** 249 (1976).
52. Dahneke, B. E., *J. Aerosol Sci.* **4,** 163 (1973).
53. Rogak, S. N., and Flagan, R. C., *J. Colloid Interface Sci.* **151,** 203 (1992).
54. Seinfeld, J. H., and Pandis, S. N., "Atmospheric Chemistry and Physics," pp. 656–699. Wiley, New York, 1998.
55. Flagan, R. C., and Seinfeld, J. H., "Fundamentals of Air Pollution Engineering." Prentice-Hall International, London, 1988.

56. Kostoglou, M., and Konstandopoulos, A. G., *J. Aerosol Sci.* **30,** Suppl. 1, s447 (1999).
57. Kostoglou, M., and Konstandopoulos, A. G., *J. Aerosol Sci.* **31,** Suppl. 1, s574 (2000).
58. Sorensen, C. M., Hageman, W. B., Rush, T. J., Huang, H., and Oh, C., *Phys. Rev. Lett.* **80,** 1782 (1998).
59. Prado, G., and Lahaye, J., *in* "Particulate Carbon" (D. C. Siegla, and G. W. Smith, Eds.), pp. 143–164. Plenum Press, New York, 1981.
60. McMurry, P. H., and Friedlander, S. K., *Atmospheric Environ.* **13,** 1635 (1979).
61. McMurry, P. H., and Friedlander, S. K., *J. Colloid Interface Sci.* **64,** 248 (1978).
62. di Stasio, S., *J. Aerosol Sci.* **32,** 509 (2001).
63. Abramovitz, M., and Stegun, I. A., "Handbook of Mathematical Functions." National Bureau of Standards, Washington, 1972.
64. Kent, J. H., and Wagner, H. Gg., *Combust. Sci. Technol.* **41,** 245 (1984).
65. Santoro, R. J., Yeh, T. T., Horvath, J. J., and Semerjain, H. G., *Combust. Sci. Technol.* **53,** 89 (1987).
66. McEnally, C. S., Köylü, Ü. Ö., Pfefferle, L. D., and Rosner, D. E., *Combust. Flame* **109,** 701 (1997).
67. Fristrom, R. M., and Westenberg, A. A., "Flame Structure." McGraw–Hill, New York, 1965.
68. Perry, R. H., and Green, D., "Perry's Chemical Engineering Handbook," VI Edition. McGraw–Hill, New York, 1988.
69. Mikhailov, E. F., and Vlasenko, S. S., *Phys. Uspekhi* **38,** 253 (1995).
70. Lin, M. Y., Lindsay, H. M., Weitz, D. A., Klein, R., Ball, R. C., and Meakin, P., *J. Phys.: Condens. Matter* **2,** 3093 (1990).
71. di Stasio, S., and Massoli, P., *Particle Particle Systems Character.* **15,** 90 (1998).
72. Narsimhan, G., and Ruckenstein, E., *J. Colloid Interface Sci.* **107,** 174 (1985).
73. Narsimhan, G., and Ruckenstein, E., *J. Colloid Interface Sci.* **104,** 344 (1985).
74. Harris, S. J., and Weiner, A. M., *Combust. Sci. Technol.* **32,** 267 (1983).
75. Prado, G., Jagoda, J., Neoh, K., and Lahaye, J., "XVIII Symposium (International) on Combustion," pp. 1127–1136. The Combustion Institute, Pittsburgh, 1981.
76. Harris, S. J., and Weiner, A. M., *Combust. Sci. Technol.* **31,** 155 (1983).
77. Kent, J. H., and Wagner, H. Gg., *Combust. Flame* **47,** 53 (1982).